Quasi-optical antennas for radiometric remote-sensing

by R.J. Martin and D.H. Martin

Millimetre- and submillimetre-wave radiometers are employed for remote-sensing of the Earth's atmosphere. They must operate in several widely-spaced frequency bands which together might exceed the fundamental bandwidth of a waveguide. A wholly independent radiometer for each band would be inefficient and considerable savings in space and weight can be achieved if all bands are received via a single aperture antenna and then separated by an optical demultiplexer, the arrangement comprising a 'quasi-optical' antenna. This paper discusses the requirements for, and the design of, quasi-optical antennas for radiometric remote-sensing and illustrates this with particular reference to the Advanced Microwave Sounding Unit AMSU-B, which was designed and built by Matra Marconi Space UK for the UK Meteorological Office and is due to be placed in orbit on a satellite in 1996.

1 Remote-sensing of the earth at millimetric and submillimetric frequencies

There are major applications for millimetre- and submillimetre-wave radiometry (30 GHz to 3000 GHz): in remote-sensing of the Earth from satellite platforms for global meteorology, oceanography and climatology; in remote-sensing of the atmosphere from balloon-borne and satellite platforms in order to monitor stratospheric chemistry; in diagnostic studies of thermo-nuclear plasmas; and in astronomy. The radiometer system in any of these applications must have a low signal throughput-loss, a high antenna beam-efficiency, and a wide overall bandwidth, and must periodically address reference sources for radiometric calibration. In most cases the antenna must scan wide fields of view. In some cases all this has to be achieved within the mass, size, thermal and other constraints of a space platform. Our purpose in this paper is to show, in the context of remote-sensing of the Earth from satellite-borne platforms, how quasi-optical antenna systems meet these demanding requirements.

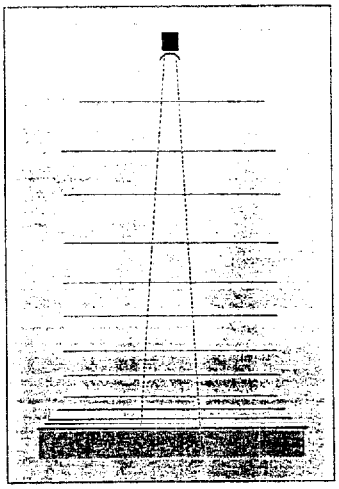

Fig. 1 A downward-looking radiometer on an Earth-orbiting satellite remotely senses thermal emission signals from the gases in a vertical column through the atmosphere and from the land or sea surface

In a radiometric measurement the thermally radiated signals from a distant source under study are collected by an antenna system and detected in several frequency-selective receivers. The strength of the signal at each measurement frequency is determined as a *radiometric equivalent temperature* (RET) for that frequency by interpolating between the signal levels measured when the radiometer's beam is filled in turn by two black-body calibration sources at differing, known temperatures.

When the Earth, with its atmosphere, is viewed by a downward-looking radiometer, as illustrated in Fig. 1, the gas in a given incremental horizontal layer of the atmosphere emits thermal radiation upwards towards the radiometer. On its way to the radiometer this signal is attenuated as it passes through successive layers. The gas in a given layer therefore influences the signal flux at the radiometer in two ways: it emits upwards its own thermal signal and it attenuates the signals emitted by all the layers below. In the millimetre-

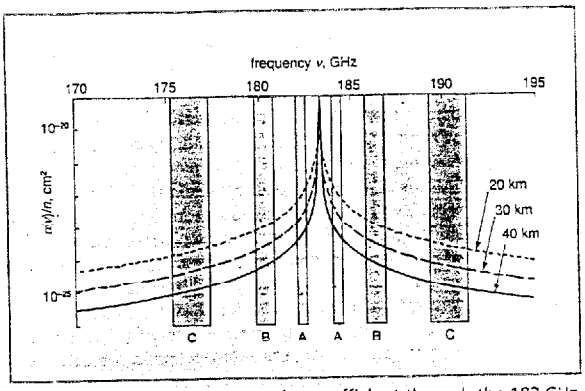

Fig. 2 Variation of the attenuation coefficient through the 183 GHz resonance of water molecules. $\alpha(\upsilon)/n$ is shown, where $\alpha(\upsilon)$ is the attenuation coefficient for n water molecules per cm^3 at T = 300K. The three curves refer to different values of total atmospheric pressure: 3 mbar (40 km altitude), 12 mbar (30 km) and 50 mbar (20 km). The frequencies of the three (double sideband) channels of the AMSU-B radiometer (labelled A, B and C) are indicated; the widths of the boxes indicate the integration bandwidths

wave range of frequencies, the emission, and the attenuation, are both consequences of resonant rotational motions of dipolar molecules in the atmosphere, especially the abundant molecules of oxygen and water-vapour.

Consider measurements made by a downward-looking radiometer over a range of frequencies within which a single rotational resonance of one molecular constituent (oxygen or water vapour) occurs. The attenuation coefficient of the atmosphere will vary with frequency in this range, having a strong peak at the molecular rotational resonance frequency — see the example in Fig. 2. It will also vary with altitude, both because it is proportional to the number density of resonating molecules, i.e. to the partial pressure of the active constituent, and because the damping of the molecular resonance due to molecular collisions broadens the peak (Fig. 2), the more so the higher the atmospheric pressure. Together with the temperature the magnitude of the attenuation coefficient for the gas in a given layer of the atmosphere also determines the upward emission from the layer.

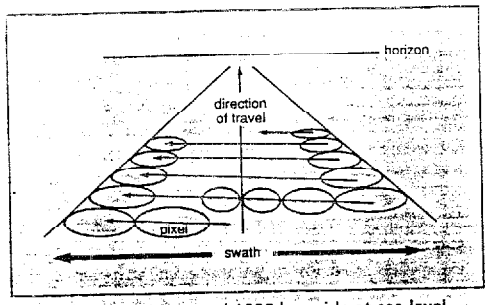

Fig. 3 The swath, around 1000 km wide at sea-level, which a downward-looking Earth-remote-sensing radiometer explores as a result of repetitive cross-track scanning of the boresight of the radiometer's antenna through about one radian

The variation of the measured RET with frequency through the molecular resonance will therefore be dependent in a complicated way on the vertical distributions of temperature and of abundance of active molecules. As the value of the attenuation coefficient is relatively large at frequencies close to the centre of the resonance the RET measured at such frequencies will usually be low because it will be determined primarily by the conditions close to the radiometer, i.e. high in the atmosphere where the atmospheric temperature is low. At frequencies well away from the centre of the resonance, on the other hand, the attenuation coefficient will be relatively low and the measured RET will consequently be relatively high since it will be determined by the conditions at low altitudes, where the temperature is higher. As the measurement-frequency is scanned through the molecular resonance, therefore, the measured RET will vary, passing through a minimum at the resonance frequency. The resonant frequencies of oxygen and water-vapour are known from laboratory measurements, as are the strengths of the resonances per molecule and the pressure dependences of the line-widths. It is therefore possible to calculate the variation of the RET with frequency for given temperature and abundance distributions.

The objective of remote-sensing, however, is the *inverse* of this, i.e. the determination of the distributions from given (measured) RETs. This is a more complicated process.[1] In fact, the temperature and abundance distributions cannot be separated by reference only to radiometric measurements in a single spectral line. For oxygen it is possible to invoke the fact that, since it is a near-perfect gas at all pertinent temperatures and pressures, it is 'uniformly mixed' in the atmosphere, i.e. its local abundance is proportional to the total local atmospheric density at all altitudes: hence, it would be possible to use radiometric measurements in an oxygen line (in practice, in a band of several closely-spaced oxygen lines) to determine the vertical distribution of atmospheric temperature. Water vapour, on the other hand, is condensible and is far from being uniformly mixed in the atmosphere. If the atmospheric temperature distribution were known from simultaneous radiometric measurements through an oxygen band, however, measurements through a water-vapour line would give the vertical distribution of water-vapour. RETs will be measured at a finite number of frequencies, of course: the larger the number, the sharper will be the resolved detail in the derived vertical distributions.

Downward-looking radiometric measurements from an orbiting satellite, over a range of millimetre-wave frequencies spanning oxygen and water-vapour resonances, thus offer the possibility of determining global vertical distributions of temperature and of water-vapour, matters of central importance in meteorology and climatology. Measurements of the RET at frequencies well

away from the molecular resonance frequencies (i.e. where the atmosphere is transparent) will relate to ocean or land surface conditions and to liquid-water concentrations in clouds and in rainfall.

Satellite-borne millimetre-wave radiometers are currently circulating the Earth and making extensive measurements in the band of closely-spaced oxygen lines near 60 GHz, at the water-vapour lines at 23 GHz and 183 GHz, and at several intermediate frequencies well away from any atmospheric molecular lines. Global maps of the vertical distributions of temperature and of water-vapour are being obtained daily, and ocean/land surface conditions and liquid-water concentrations in clouds and in rainfall are being monitored continuously. New millimetre-wave remote-sensing systems are under development which will have better vertical resolutions and will cover greater ranges of altitude.[1]

A radiometer collects signal power from the atmosphere within a tapered column around the line-of-sight of the antenna (Fig. 1) and therefore directly resolves in the horizontal plane. The antennas of early satellite-borne radiometers gave resolutions of about 100 km at ground level but future systems will operate at higher frequencies and will provide resolutions of a few kilometres in order to resolve various important types of meteorological structure on that scale. For this it will be necessary to achieve antenna patterns which are closely matched over the full operating frequency range, with extremely high beam-efficiency, typically in excess of 95% within about 1° or less of the boresight.

For meteorological purposes it is necessary to cover most of the earth's surface at least once in every 24 hrs. To achieve that with a radiometer on a polar-orbiting satellite, the antenna must scan repeatedly over an angular range of 60° or more, transversely to the line of orbital motion (Fig. 3), in order to sweep out a swath at the surface about 1000 km wide; each such traverse has to be completed within the time taken for the satellite to move forward through one spatial-resolution interval. For this reason, with a radiometer having high spatial resolution, the scan time must be no more than a few seconds, and each radiometric datum must be taken in no more than a few tens of milliseconds of integration time.

Radiometric calibration involves directing the radiometer at two reference sources in turn: each source must be black (i.e. wholly absorbing) for incident thermal power, and at constant uniform temperature. One of these may be the external cosmic background in a direction away from the Earth, at a temperature of 3K, and the other an on-board cavity at local ambient temperature. The calibration steps are interleaved with the remote-sensing scans (Fig. 4).

Our concern has so far been with downward-looking radiometers. There is another important remote-sensing method, known as limb-sounding, in which the radiometer is directed towards the horizon (Fig. 5) and vertical distributions are explored by scanning in elevation angle. This method is well-suited to the study of molecular constituents in and above the stratosphere, including those that are involved in the reactions that affect the ozone

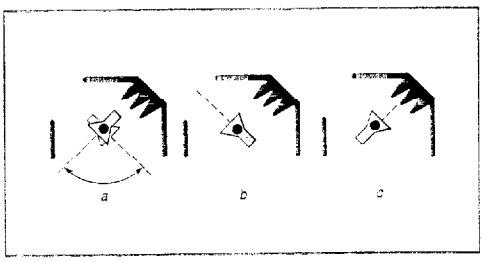

Fig. 4 The measurement cycle of a satellite borne radiometer: (a) the radiometer's antenna is first swept through about one radian across the downward-looking vertical to measure the Earth's emission signal, (b) it is then directed into the deep-space background to provide one of two calibration points; (c) in the last step in the cycle the antenna is directed into an on-board black cavity to provide the second calibration point. The cycle lasts no more than a few seconds and the cycle is repeated continuously

layer.[2] Most of these molecules have rotational transitions which give rise to absorption lines in the submillimetre-wave range and radiometric measurements at the frequencies of these lines can serve to determine their vertical distributions. For a line-of-sight at stratospheric altitude or above, the low pressures result in very narrow line-widths for all molecular lines. For this reason, there are some narrow but clear gaps between the great number of submillimetre-wave water-vapour, oxygen and ozone lines in which there are lines of the minor constituents. Vertical distributions of ozone, ClO, HNO_3, and H_2O_2 are already being determined by limb-sounding from satellite platforms in bands at 63 GHz, 183 GHz, and 205 GHz. Many other molecular species have been assessed by limb-sounding radiometry from high-altitude balloon-borne platforms at frequencies up to 3000 GHz. Global studies of a number of these (OH, HCN, OClO, HCl, BrO, HBr, N_2O, NO, etc.) will be major objectives for future space-based systems.

In a limb-sounding measurement the radiometer's

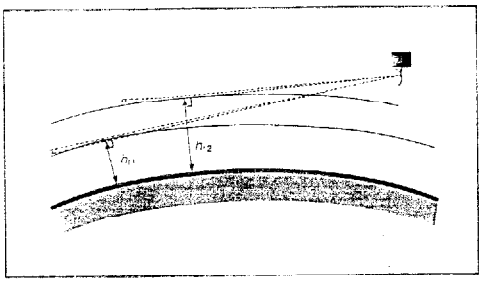

Fig. 5 A limb-scanning radiometer, on an Earth-orbiting satellite or a high-altitude balloon-borne platform, remotely senses thermal emission signals from molecular species along the line-of-sight of the radiometer, with a weighting function having a broad peak centred at the tangent point, at altitude h_t. A change in elevation angle of the radiometer results in sounding at a different altitude, but at a point displaced horizontally

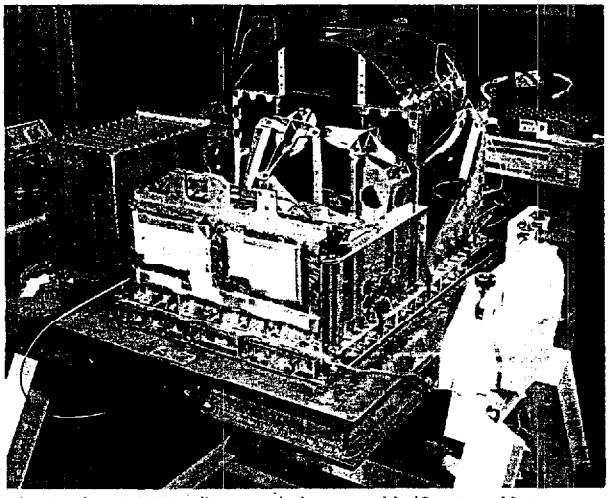

Fig. 6 The AMSU-B radiometer during assembly (Courtesy: Matra Marconi Space UK Ltd.)

line-of-sight passes through points having all values of altitude $h \geq h_t$, where h_t is the altitude at the tangent-point (Fig. 5), but the received signal power derives mainly from the portion within about 140 km to each side of the tangent point, which spans a 1·6 km range of altitude. Since the distance from the radiometer to the tangent point will usually exceed 1000 km, the angular resolution which will match the 1·6 km is less than 0·05°, which is a challenging requirement in the design of the antenna. The limb-sounding method provides the long emissive path-lengths necessary if molecular species of low abundance (but of major climatological and environmental consequence) are to be detected, but it allows only a limited horizontal resolution in the line-of-sight; the vertical resolution is good, however, and that allows the crucial vertical abundance distributions to be measured.

2 AMSU-B: a remote-sensing radiometer

Before explaining how quasi-optical antenna systems can be designed to meet the demanding antenna performances required in earth-remote-sensing an example of a radiometer will be described. The 'Advanced Microwave Sounding Unit' (AMSU) is a millimetric radiometer system which will be carried on an NOAA (the American National Oceanographic and Atmospheric Administration) satellite to be launched in 1996 into a sun-synchronous polar orbit. It has two radiometers: AMSU-A and AMSU-B. The former will operate in the 23 GHz water-vapour line, in the 50–60 GHz group of oxygen lines, and in an atmospheric window at 89 GHz. AMSU-B (Fig. 6) will operate in the atmospheric windows at 89 GHz and 150 GHz, to map precipitation and other surface conditions, and in the 183 GHz water-vapour line to determine water-vapour vertical distributions, as outlined in Section 1. The AMSU-B radiometer will be described here. It has been developed at Matra Marconi Space UK, Bristol (formerly British Aerospace Space Systems) for the UK Meteorological Office.

Table 1 lists the major performance specifications which were set for the AMSU-B antenna and its feed.

The quasi-optical system designed to meet these requirements[2,3] is illustrated in Fig. 7. A dual-offset reflector antenna is followed by a quasi-optical frequency-demultiplexer in which two planar dichroic frequency-filters split the incoming broadband signal beam into three separate beams (Fig. 8), the first covering the 86–92 GHz band, the second the 148–152 GHz band, and the third the 175–191 GHz band; each of these beams is finally condensed into a waveguide feed-horn. The optics of the 183 GHz channel is illustrated schematically in Fig. 9 (two plane reflectors which fold the optical path are omitted from this diagram); the optics in the other channels are similar. The structural form of the demultiplexer, which incorporates six ellipsoidal and two plane reflectors, is illustrated in Fig. 10.

The feed-horns for the 89 GHz and 150 GHz bands are linearly-tapered conical corrugated horns[4] which admit axially-symmetric plane-polarised signal beams. For the particularly wide band at 183

Table 1: Summary of AMSU-B requirements

Frequency bands, GHz	87·6 – 90·4 148·8 – 151·4 175·31 – 191·31	
Full width half-power (FWHP) angle	1·1° ± 10%	all channels
Beam efficiency	≥95%	within cone equal to 2·5 times average FWHP
	≥98%	within cone whose included angle is 4°
Insertion loss	≤1·4 dB	all channels
In-band ripple	≤0·5 dB	all channels
Crosspolar relative to copolar peak	≤–27 dB	all channels
Sidelobe levels	≤–27 dB	all channels
Scanning	±49° about nadir 18 ms per pixel	continuous, cross-track
Calibration: cold	3 space views	through antenna
hot	on-board target	through antenna

GHz, the horn is shaped (Fig. 11) in such a way that, at all frequencies within the band, the field over the aperture plane has a uniform phase; this is required in order to achieve close matching of the antenna patterns for all frequencies within the band. The surface quality and the sizes of the reflectors are such as to assure extremely low throughput-loss throughout each band (see the in-band ripple requirement given in Table 1). $< 0{\cdot}5\,dB$

Each beam, once collected by its feed-horn, is transported in a short length of waveguide to the mixer of a receiver. Local-oscillator power, at the centre-band frequency, is delivered to the mixer from an in-guide solid-state source. The intermediate-frequency bandwidth is 1 GHz for the 89 GHz and 150 GHz receivers. The 183 GHz receiver has intermediate-frequency filters to split the band into three double-sideband output signal channels centred on 183·3 ± 1·0, 183·3 ± 3·0, and 183·3 ± 7·0 GHz, with bandwidths of 0·5, 1·0, and 2·0 GHz, respectively (see Fig. 2).

The signal beam emerging from the primary of the dual-reflector antenna is at 90° to the incident beam (Fig. 9) and rotation of the primary around the axis of the emergent beam (with the rest of the radiometer stationary) provides the required ±49° scan on the Earth and the two calibration views, i.e. the cold space background and an on-board ambient-temperature blackbody cavity (Fig. 4).

The optical design process for this radiometer required the hierarchy of analytical and computational methods examined in the following Section. An indication of the quality of these design methods in given in Fig. 12, which shows the agreement between the system's 183 GHz antenna patterns as calculated in the design process and as subsequently measured with the final radiometer; the patterns shown here are for the most demanding cases with the antenna at the extreme of the scan, 49° off nadir.

3 Long-wave optics and quasi-optical antennas

A high-gain millimetre-wave receiving antenna comprises two or more shaped reflectors in tandem which progressively reduce the width and directivity of the incoming signal beam so that it finally couples efficiently into the feed-horn of a waveguide. A remote-sensing system must operate in several widely-spaced frequency bands which together might exceed the fundamental bandwidth of a waveguide. That might suggest that a wholly independent radiometer should be provided for each band. However, there would be considerable saving of space and weight if the signal beams for the several bands were all received via a single aperture antenna and then separated by a demultiplexer after some reduction in beamwidth. Such demultiplexing could in principle be done after the wideband beam has been condensed into overmoded waveguide, but it is not possible to condense efficiently, into a single (overmoded) waveguide, incoming beams which have equal areas and angular widths but widely different frequencies. Moreover, use of overmoded guide would risk both loss of high beam-efficiency due to mode-conversion and radiometric error associated with high throughput losses. The demultiplexing must be done optically, i.e. with beams propagating in free-space (before being condensed into waveguide), if very low throughput loss and precisely matched antenna patterns over an extremely wide overall bandwidth are required.

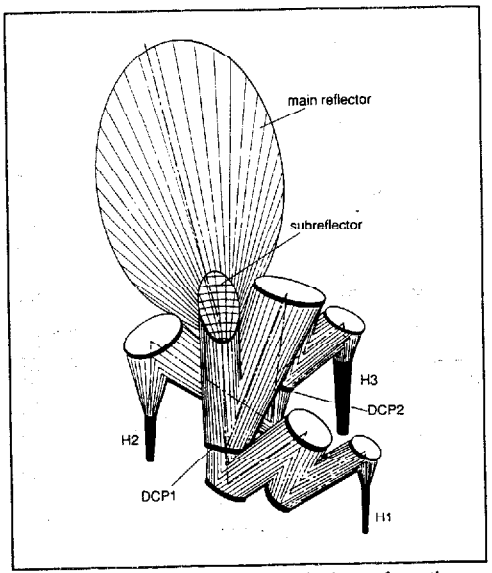

Fig. 7 In the AMSU-B radiometer the beam from the dual-offset antenna (main and subreflector) passes via collimating reflectors, the dichroics DCP1 and DCP2 (at which the beam is divided into three frequency bands) and condensing reflectors (which concentrate each of the three beams) to three feed-horns with receivers (H1 for 175–191 GHz, H2 for 148–152 GHz, H3 for 86–92 GHz)

Note that the feed-horns of the receivers of such an antenna system are the beam-defining components. The signal beam that any antenna system will wholly admit in reception is identical in form, apart from time-reversal, to the beam that it would generate in transmission if the in-guide detector were replaced by an in-guide source (the

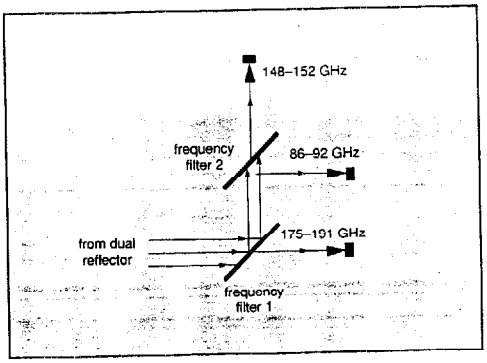

Fig. 8 Schematic representation of the separation of a signal beam into the three AMSU-B bands using two planar dichroic plates. Each plate transmits, with little loss, the signal power in one band and reflects that in the other bands

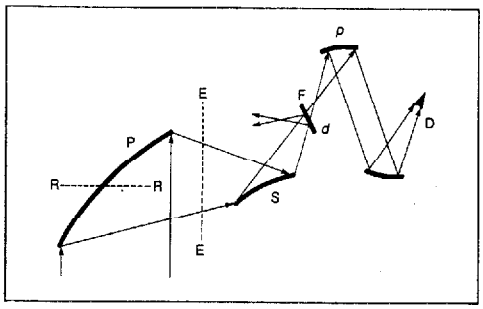

Fig. 9 A single channel of the AMSU-B radiometer. A downward-looking dual-reflector antenna, with off-axis paraboloidal primary reflector P, and off-axis hyperboloidal secondary reflector S, brings the rays representing an incoming signal beam to a beam-waist at F; the beam diverges from the beam-waist and is quasi-collimated by an ellipsoidal reflector *p*, and focused by a further ellipsoidal reflector into a receiver feed-horn at D. A planar dichroic frequency-filter *d* splits off the signal power into the other bands. The antenna is scanned by rotating the primary reflector around the axis RR, while keeping the system to the right of line EE fixed

fundamental reciprocity property). It is usually more straightforward to determine the form of the transmit/receive beam for a particular antenna by considering transmission rather than reception, even when the latter process is the one of interest. Knowledge of the modes that propagate through a feed-horn from an in-waveguide source allows the form of the field of the transmit beam over the aperture plane of the horn to be determined. Optical theory can then be used to determine the form of the beam as it propagates away from the horn, through the optical demultiplexer and reflector antenna and into the far-field. The whole of the optical train in front of the feed-horn, including the optical demultiplexer, clearly must be seen as an antenna, a 'quasi-optical' antenna.

The theorems in optical theory known collectively as Fourier optics refer to signal beams propagating through systems of 'ideal lenses'. An 'ideal lens' increments the phase of the field of a signal beam as it passes through by an amount which is quadratic in the off-axis distance r, i.e. $\Delta\phi = (4\pi/f)r^2$, where the constant f is known as the focal length of the lens; it does this without modifying the beam's amplitude distribution. We will start by applying optical theory to the ideal lens system shown in Fig. 13, which is optically equivalent to the radiometer channel of Fig. 9.

The first theorem of Fourier optics[3] states that the field in the back focal plane of an ideal lens (i.e. the plane located at distance f behind the lens, see Fig. 14*a*) is the two-dimensional Fourier-transform of the field in its front focal plane (the plane at distance f in front), the transform variables being $\{x_f, y_f\} \rightarrow \{(k/f)x_b, (k/f)y_b\}$, where $\{x_f, y_f\}$ are the Cartesian co-ordinates in the front focal plane, and $\{x_b, y_b\}$ are co-ordinates in the back focal plane (k is $2\pi v/c$, where v is the signal frequency and c is the velocity of light).

Consider now two ideal lenses separated by the sum of their focal lengths so that the back focal plane of the first reflector coincides with the front focal plane of the second (see Fig. 14*b*); this is known as a *confocal pair*. By the first theorem of Fourier optics, the field in the back focal plane of the second lens of the pair is derived from that in the front focal plane of the first by two successive Fourier transformations. Such a double Fourier transformation has a very simple outcome: the initial function is regained with inversion through the axis and with co-ordinates scaled by the ratio of the two focal lengths. That is to say, the field in the back focal plane of the second reflector of a confocal pair is an inverted *coherent image* of the field in the front focal plane of the first, with a magnification factor equal to the ratio of the focal lengths. This is the case *independent of frequency*, and confocal designs are for this reason important when wideband performance is required.

The first theorem of Fourier optics was stated above in the context of a single lens but it applies also to any non-confocal train of lenses. It is necessary, of course, to identify the front and back focal planes of the train, and to determine its focal length in terms of the focal lengths and separations of the constituent lenses. For the two-lens case

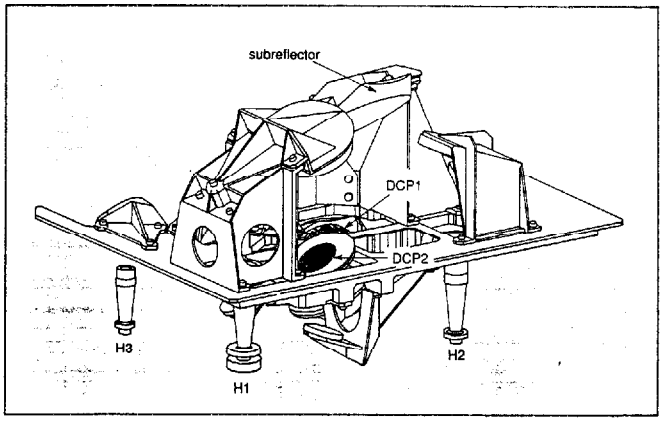

Fig. 10 Configuration of the reflectors and dichroic frequency-filters, with their mounting frames, and the receiver feed-horns in the AMSU-B demultiplexer

these are easily stated, as given in Fig. 15.

A further Fourier optics theorem relates the near-field of a paraxial free-space signal beam to its far-field; specifically, the directional variations of amplitude and phase in the far-field are given by the Fourier transform of the signal beam's field over a cross-sectional plane in its near-field, the transform variables being $\{x_n, y_n\} \rightarrow \{k_x, k_y\}$, where $\{x_n, y_n\}$ are the Cartesian co-ordinates for the near-field plane, and $\{k_x, k_y\}$ are the wave-vector components for the far-field; $k_x \equiv k\sin\theta\cos\phi$ and $k_y \equiv k\sin\theta\sin\phi$, where θ, ϕ are polar co-ordinates with respect to an origin in the near-field plane.

We can now determine the main optical function of the ideal-lens radiometer channel illustrated in Fig. 13. First note that lenses 4 and 3 form a confocal pair, and the feed-horn's aperture is in the front focal plane of the first (lens 4); consequently, the field in the back focal plane of the second (lens 3) is a *coherent image* of the field in the aperture plane of the feed-horn. Secondly note that the back focal plane of lens 3 is coincident with the front focal plane of the dual-lens antenna (lenses 2 and 1, a non-confocal pair) so that, in moving from that plane through the dual-lens antenna to its back focal plane, there is a Fourier transformation of the field; and there is a *second* Fourier transformation in going from there to the far-field, so there is another coherent imaging process. The channel as a whole thus produces a far-field in which the directional variations of amplitude and phase are a copy of the spatial variations of amplitude and phase over the aperture of the feed-horn. This is summarised diagramatically in Fig. 16. The far-field is obtained simply by replacing the Cartesian co-ordinates, x_h and y_h, in the expression for the field over the horn-aperture with $(f_3/f_4)f\sin\theta\cos\phi$ and $(f_3/f_4)f\sin\theta\sin\phi$, respectively, where f is the focal length of the dual-lens antenna, i.e. $f = (f_1 f_2)/(f_1 + f_2 - d)$.

Since the field distribution in the aperture of a feed-horn is the same for all frequencies over the bandwidth of the horn, and falls sharply to zero at the edges of the aperture, a confocal antenna system will therefore produce nearly identical antenna patterns, of very high beam-efficiency, at all frequencies within a wide band. This is exactly what is required for remote-sensing. If the aperture of the feed-horn is circular with radius a, the frequency-independent off-axis angle, θ_a, at which the far-field antenna-pattern falls sharply to zero is

$$\sin\theta_a = \left(\frac{f_3}{f_4}\frac{1}{f}\right)\frac{1}{a} = \left(\frac{f_1+f_2-d}{f_1 f_2}\,\frac{f_3}{f_4}\right)\frac{1}{a}$$

This relates the required θ_a to the focal lengths of the reflectors and the aperture of the feed-horn in a channel.

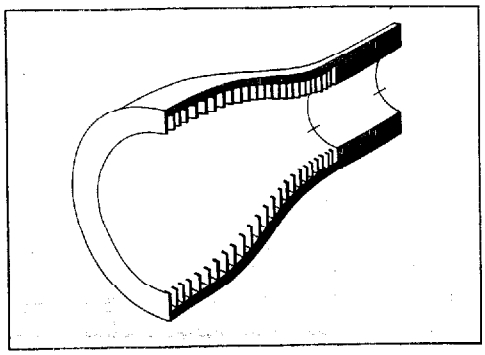

Fig. 11 Cut-away diagram of a shaped corrugated feed-horn. Such a horn produces an axially-symmetric field with uniform polarisation *and uniform phase* over its aperture plane

So far the use of Fourier optics has been described in the context of a system of ideal lenses. A conic-section reflector (paraboloidal, ellipsoidal or hyperboloidal), used on-axis, approximates fairly closely to ideal-lens behaviour in that it essentially gives a quadratic phase-increment to a signal

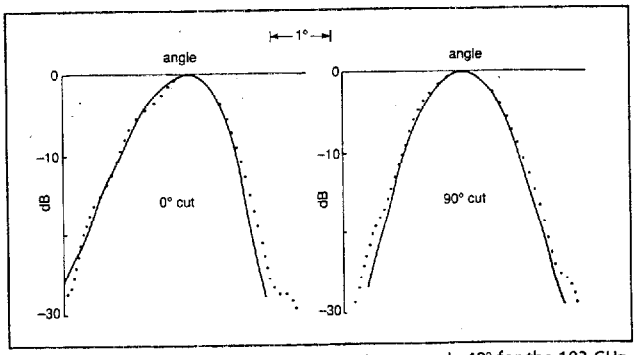

Fig. 12 Measured (....) antenna patterns at scan angle 49° for the 183 GHz channel of AMSU-B compared with the theoretically (——) determined design patterns

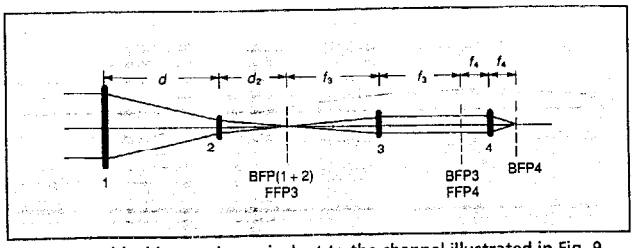

Fig. 13 An ideal-lens train equivalent to the channel illustrated in Fig. 9. The lenses are numbered 1 to 4. The spacing of the confocal pair 1 and 2 is specified in terms of their focal lengths. The vertical broken lines indicate back and front focal planes; the distance d_2 to the back focal plane of the dual-lens (1 and 2) is as given in terms of f_1, f_2 and d in Fig. 15. The front focal plane of the dual-lens is not shown; it is to the left of lens 1, at distance d_1 as given in Fig. 15

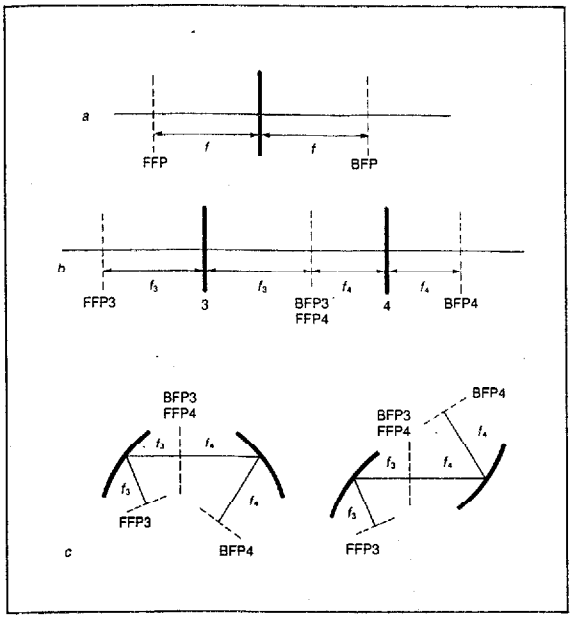

Fig. 14 Locations of front focal planes (FFP) and back focal planes (BFP) (*a*) for a single lens of focal length *f*, (*b*) in a confocal pair of lenses (labelled 3 and 4), (*c*) in a confocal pair of off-axis paraboloidal reflectors, in two configurations

beam reflected from it; the magnitude of this quadratic increment serves to define a focal length for the reflector just as for an ideal lens. When such a reflector is used off-axis (Fig. 17) it provides, additionally, a linearly tapered phase-increment, but that simply gives rise to the change in direction of propagation of the emergent beam relative to the incident beam. The quadratic increment determines the focal length, *f*, of the reflector. Fig. 17 gives *f* in terms of the geometrical parameters of the conic section.

Front and back focal planes can therefore be defined for conic-section reflectors as for lenses, and all the results established above for ideal-lens systems will carry over to

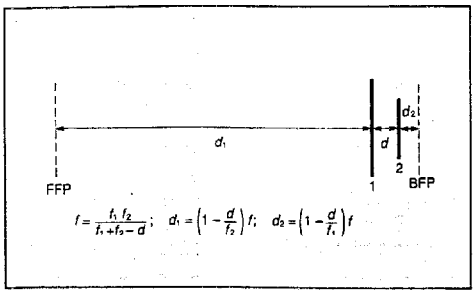

Fig. 15 Locations of the front and back focal planes (FFP and BFP respectively) of a nonconfocal system of two lenses, of focal lengths f_1 and f_2, and of separation d. The dimensions ($f_1 = 1{\cdot}25\,d$ and $f_2 = -0{\cdot}4\,d$) correspond to those of the AMSU-B dual reflector, but the formulae apply for all dimensions

equivalent reflector systems. In particular, a radiometer channel comprising conic-section reflectors in the configuration shown in Fig. 9 (as used in AMSU-B, for example) is equivalent to the lens system of Fig. 13 and will have the same advantageous performance characteristics.

Though the main characteristics of a confocal radiometer channel are thus established using Fourier optics, a number of important design parameters remain to be decided since the Fourier optics provide no information on the field distributions in cross-sections other than focal planes, in particular in the planes of the reflectors. In designing an antenna system it is important to know the spread of the fields at the reflectors in order to ensure that the reflector diameters are made large enough to avoid significant beam truncation, which would have two undesirable consequences, namely radiometric error due to the implied detection of thermal emission from the interior of the radiometer and the generation of sidelobes in the far-field antenna pattern with consequent loss of beam efficiency.

The method of *beam-mode analysis*,[5] in which a free-space signal beam is decomposed into independently propagating modes, can be used to determine the field in any cross-section through a beam. A beam-mode maintains the same mathematical form in all transverse cross-sections as it propagates but with a progressively increasing scale (this is diffractive spreading of the mode arising from its finite width). A beam-mode's field has a spherical phase-front in every cross-section, so the passage of a mode through an ideal lens or conic-section reflector is a simple matter of a discretely-changed phase-front curvature. The changing values of the scale parameter, of the phase-front curvature, and of the phase of a mode as it propagates through a system can be readily computed using simple transfer matrices for free-space steps and passages through ideal lenses.[5]

The relative amplitudes of the modes making up a beam are determined by fitting to the known field in the aperture of the feed-horn. Once this has been done, the full form of the beam's field in any chosen cross-section (at a reflector, for example) can readily be determined by superposition of the modes' fields there. A moderate number of (low-order) modes suffices to give a close fit to the field produced by a corrugated feed-horn and quite modest computations are involved.[6]

As an illustration of the results of such analysis, Fig. 18 shows the variation of the width parameter of a beam, w, as it propagates through the optical train illustrated in Fig. 13, taking values for the focal lengths and spacings of the lenses, and for the dimensions of the feed-horn, from AMSU-B's 89 GHz channel (upper Figure) and 183 GHz channel (lower Figure). w is simply the width parameter of the Gaussian function that most closely fits the calculated

field distribution in each cross-section. The actual field distributions are not exactly pure Gaussian functions, of course; the detailed forms are shown in Fig. 19, where the field amplitude is plotted against r/w, where r is the off-axis distance and w the width parameter. The variable 2Θ used in this Figure is related to the down-beam distance in a rather complicated way:[6] it will suffice here to note that all down-beam distances are included within the span of 2Θ included in the Figure, and that the values of 2Θ that correspond to the locations of the reflectors in the 183 GHz channel are as indicated along the bottom of Fig. 18 and the detailed forms of the fields at the reflectors in this channel can therefore be seen in Fig. 19 at those values of 2Θ.

The reflectors in AMSU-B have diameters sufficient for the truncation to be of negligible consequence (about 4 × the width parameter) as indicated by the vertical lines at the locations of the lenses in Fig. 18). The main reflector for the 89 GHz beam is an exception to this; for this channel, the specification on sidelobe levels gave room for some degree of truncation.

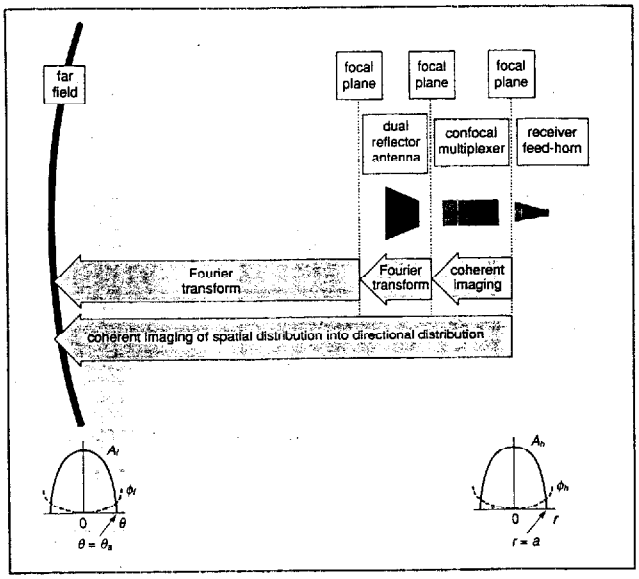

Fig. 16 Schematic description of the successive transformations suffered by a signal beam as it propagates through a radiometer channel, from the receiver feed-horn on the right into the far-field at the left *via* a confocal multiplexer and antenna. The broad arrows indicate the field transformations involved in moving from one focal plane to the next. The bottom arrow indicates the overall transformation effected by the whole system, namely a mapping of the distribution of the field over the horn's aperture (small diagram on the right) into a far-field directional distribution of identical form (small diagram on the left)

Note also that a conic-section reflector used off-axis does not behave exactly as an ideal lens — it will introduce some aberrations in the phase and amplitude distributions (i.e. terms of higher order than quadratic), and some crosspolar contamination. Such aberrations are greater the larger the reflector's off-axis distance and the greater the divergence of the beam incident on the reflector.[7] Minimising those factors in the course of a lay-out design will usually lead to increased instrument volume unless plane reflectors can be included to fold the beam (as in the 183 GHz channel of AMSU-B). It is therefore important to recognise that an educated selection of the symmetry in a configuration of two or more off-axis reflectors can result in the aberration produced by one reflector being largely cancelled by that due to the next. For example, of the two configurations of a pair of off-axis reflectors shown in Fig. 14*c*, that on the left will produce a much lower degree of aberration than that on the right if the reflectors are near to being paraboloids (so that the beam between the two is quasi-collimated); the reverse will be the case, however, if the reflectors are such that a small beamwaist (focus) is formed between the reflectors. Such minimising of overall aberration by choice of configuration is an important part of the design process for a high-performance radiometer; it determines in particular the detailed form of the main dual reflector antenna.[8]

Once an optical design which meets the performance specifications has been achieved analytically, as outlined above, confirmation that the aberrations and losses due to beam truncation have been contained within acceptable limits can be sought through numerical, finite-element, evaluations of diffraction integrals. The codes required for multireflector systems are complex and extremely demanding in computer capacity and time, and such computations are only undertaken when a system design in which there can be a high degree of confidence has been achieved.

4 Frequency demultiplexers

The dichroic plates used for the frequency-demultiplexing (Fig. 8) must reflect the signal power within one band and transmit that in the remaining bands, and must do so with high efficiencies (< 0·5 dB loss) to avoid unacceptable levels of radiometric error.

The dichroic plates used in AMSU-B are waveguide-arrays in the form of parallel-sided metal plates perforated by regular arrays of closely-spaced circular holes (Fig. 20*a*). Provided the incident signal beam has sufficient width to illuminate many individual waveguides in the array, such a plate functions as a lowpass filter in reflection and as a high-pass filter in transmission, and the transition frequency in both cases is close to the cut-off frequency of the individual waveguides. An upper bound to efficient transmission is set by the frequency above which diffraction from the array into grating lobes can occur. The third

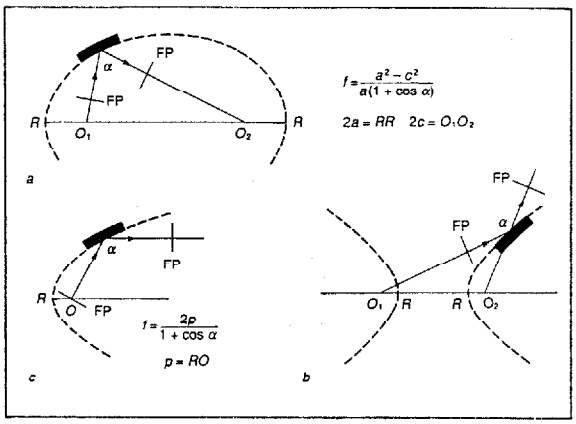

Fig. 17 The reflecting face of an off-axis reflector is a portion of the surface generated by rotating a conic section about its axis. The broken lines in the Figure indicate such surfaces: an ellipsoid in (*a*), a hyperboloid in (*b*), and a paraboloid in (*c*), with axis of rotation *RR* in each case. The shaded region represents a section through the reflector. The points denoted by *O* in each case are the geometrical foci of the conic section and the arrowed lines indicate the directions of incidence, and of emergence, of signal beams at the reflector. The focal length of a reflector, *f*, is determined by the angle through which the beam is deflected by the reflector, α, and by the geometrical parameters of the conic section, i.e. *a* and *c* for both the ellipsoid and the hyperboloid, and *p* for the paraboloid. The formula at top right gives *f* for an ellipsoidal or hyperboloidal reflector (*f* takes a negative value for the latter since, for that case, *a* is smaller than *c*); the formula in (*c*) gives *f* for a paraboloidal reflector. FP indicates the location of a focal plane, at distance *f* from the reflector

characteristic frequency for the plate is that corresponding to resonance in the length of the guides. Careful selection of the dimensions when designing such a dichroic plate will sequence these three frequencies so that the transition from high reflection to high transmission, as the signal frequency increases, is sharp, and so that the high transmission is maintained over a usefully wide band. There is a basic limit to the transmission bandwidth arising from the fact that the spacing in the array must exceed the diameter of the waveguides. This limit is tighter the larger the angle of incidence onto the dichroic plate (because diffraction effects become significant sooner). Large angles of incidence are desirable when the available volume for an instrument is limited, so this can be a deficiency of waveguide-array dichroic plates.

Better in this regard, and also with respect to quality achieved in manufacture for frequencies in the terahertz range, are dichroics made up as stacks of frequency-selective surfaces (FSSs).[9] Each FSS is a regular array of thin-film metallic elements formed lithographically on a thin low-loss dielectric substrate, or the inverse of this, i.e. an array of shaped apertures in a metallic film on a substrate (Figs. 20*b–d*). Higher reflectances and transmittances, and wider bandwidths, than can be achieved with a single FSS are usually required, so two or more FSSs in a multilayer stack must be used. With careful selection of the spacings between successive FSSs, multipass resonances greatly sharpen the transitions from high reflection to high transmission; a balance has to be struck between the sharpness of the transition and the depth of ripple of the transmission coefficient across the transmit band. There is a close correspondence between the design principles of such optical filters and those of filter networks used at lower frequencies.

Methods of modal analysis which determine the changes with frequency and angle of incidence of the amplitude and phase imposed on a plane-wave signal when it is reflected from, or transmitted through, such dichroic plates are now well-developed[9] (Fig. 21). They invoke translational symmetries appropriate to an infinitely wide plate and to a truly plane (and therefore infinitely wide) incident signal beam. A real beam is of

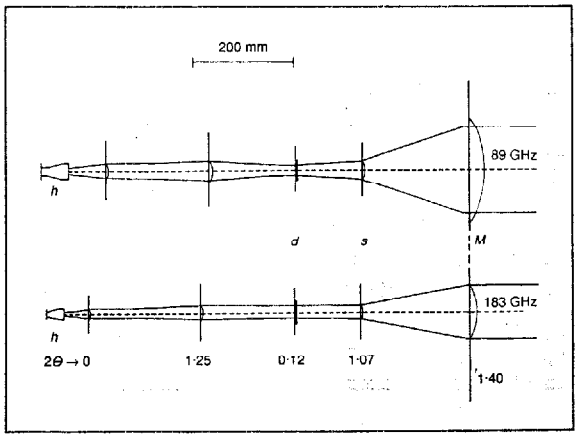

Fig. 18 Variation of the width parameter (half the distance between the pair of thin lines running from left to right) of a beam passing through an optical train; the upper train has the same reflector separations and focal lengths as the 89 GHz channel of AMSU-B and the lower the same as the 183 GHz channel. *M* denotes the main reflector, *s* the subreflector, *d* the dichroic frequency filter, and *h* a feed-horn; *d*,*s* and *M* are common to the two channels. The diameters of the reflectors and dichroic are indicated by the vertical lines. The values for 2Θ shown along the bottom of the Figure relate to Fig. 19

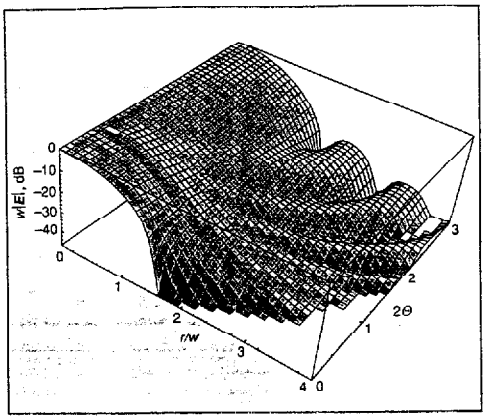

Fig. 19 Patterns of field-amplitude over cross-sections through a propagating beam. The patterns for the cross-sections at the reflectors in the 183 GHz channel of AMSU-B are those at the values of 2Θ indicated under the reflectors in Fig. 18. Note that the field amplitude is plotted here against a reduced off-axis distance r/w, where r is the off-axis distance and w is the width parameter of the beam (see text)

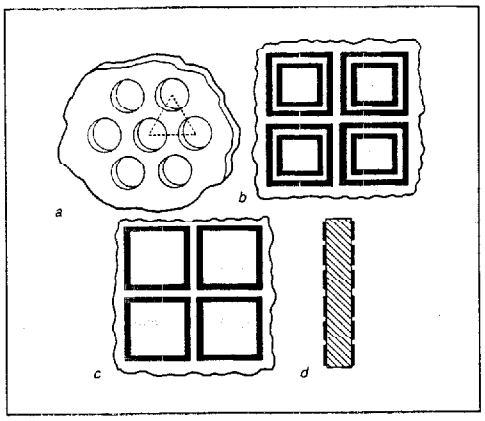

Fig. 20 (*a*) A small portion of a waveguide-array dichroic frequency-filter. (*b*), (*c*) Examples of printed patterns used in frequency-selective surfaces. (*d*) Forming FSS layers on the faces of a low-loss dielectric slab, as illustrated here, gives enhanced dichroic performance (see Fig. 21)

finite width, however, but it can be viewed as a superposition of (infinitely wide) plane waves spanning a range of forward directions of propagation; the localisation of the beam is a consequence of interference between the constituent plane waves.[5] This makes it possible to use the plane-wave dichroic properties to calculate the effect of introducing a finite dichroic into a beam of finite width. The directional distribution of the plane waves which constitute a beam of finite width is given by the Fourier transform of the field over any transverse cross-section of the beam;[5] clearly, therefore, the angular spread of the constituent plane waves will be smaller for a wide beam than for a narrow beam. An important requirement in designing the demultiplexer of a radiometer system is to ensure that the signal beam at a dichroic plate has sufficient width that this spread does not exceed the range of angles of incidence over which the dichroic plate maintains a high performance level.

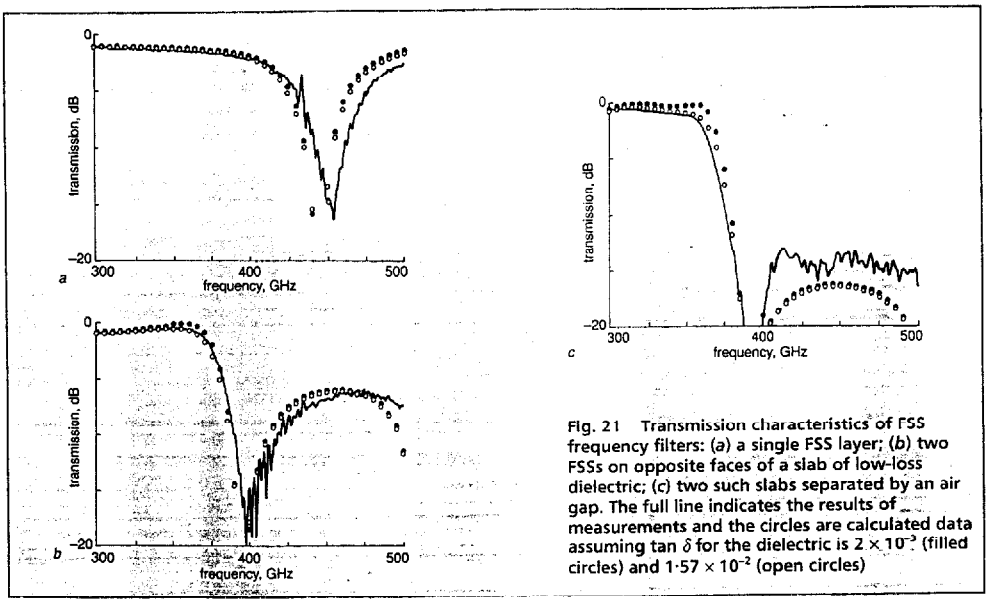

Fig. 21 Transmission characteristics of FSS frequency filters: (*a*) a single FSS layer; (*b*) two FSSs on opposite faces of a slab of low-loss dielectric; (*c*) two such slabs separated by an air gap. The full line indicates the results of measurements and the circles are calculated data assuming tan δ for the dielectric is 2×10^{-3} (filled circles) and $1{\cdot}57 \times 10^{-2}$ (open circles)

5 Future directions

Future space-borne downward-looking millimetre-wave remote-sensing radiometer systems will sharpen the spatial resolutions achieved in mapping the major meteorological atmospheric parameters, in both horizontal and vertical planes; the latter will require extensions of the number of frequencies sampled through the molecular resonances, and the former will require larger antennas and, eventually, imaging feed-arrays.

The imminent advances will be in moving to higher frequencies, well into the terahertz range, particularly for limb-sounding studies of molecular species involved in stratospheric chemistry. For example, currently under development are the European Space Agency's MASTER and SOPRANO instruments. MASTER will cover four millimetre-wave bands (199–207 GHz, 296–306 GHz, 318–326 GHz and 342–348 GHz) within which occur molecular resonances of water, ozone, oxygen, carbon monoxide, and various oxides of nitrogen. SOPRANO will operate in three submillimetre-wave bands (498–503 GHz, 624–638 GHz and 951–956 GHz) in which there are resonances of ClO, BrO, HCl, CH_3Cl, and NO. The antennas for these instruments will be appreciably larger than that of AMSU-B — approximately 2·2 m for MASTER and 1 m for SOPRANO.

Optical (rather than waveguide) delivery of the local-oscillator power to the mixers of receivers will become necessary at the higher frequencies. Planar wire-grids can be used as polarising directional couplers and can be configured together to form four-port devices which efficiently overlay signal and local-oscillator beams, or to serve as single-sideband filters. In fact, optical networks can be designed to perform a great variety of signal-processing functions in ways analogous to the network approaches to signal processing familiar in other ranges of frequency.[10] The processing of signal beams in optical networks will clearly be a growing feature in submillimetre-wave radiometer design.

Acknowledgments

We wish to express our thanks for helpful discussions on this paper to Rob Andrewartha, Janet Charlton, Mark Jarrett, Mike Wragg, John Hall and Robert Cahill of Matra Marconi Space UK Ltd., and to the UK Meteorological Office and Matra Marconi Space UK Ltd. for permission to include Figures and data on AMSU-B. Richard Wylde of Thomas Keating Ltd. kindly made available to us the analyses of beam-forms given in Figs. 18 and 19.

References

1 JANSSEN, M.A. (Ed.): 'Atmospheric remote sensing by microwave radiometry' (John Wiley, 1993)

2 MARTIN, R.J., and HALL, W.J.: 'Quasi-optical triplexing feed for AMSU-B radiometer'. 8th Int. Conf. on Antennas and Propagation, ICAP93, 30th March–2nd April 1993, Edinburgh, UK, IEE Conf. Publ. No. 370, Vol. 2, pp. 930–933

3 MARTIN, R.J.: 'The AMSU-B quasi-optics'. ESA Workshop on Millimetre-wave Applications and Technology, ESTEC Noordwijk, 5th–7th December 1995

4 CLARRICOATS, P.J.B., and OLVER, A.D.: 'Corrugated horns for microwave antennas' (IEE, London, 1984)

5 MARTIN, D.H., and BOWEN, J.W.: 'Long-wave optics', *IEEE Trans.*, 1993, **MTT-41**, pp. 1676–1690

6 WYLDE, R.J., and MARTIN, D.H.: 'Gaussian beam-mode analysis and phase-centres of corrugated feedhorns', *IEEE Trans.*, 1993, **MTT-41**, pp. 1691–1699

7 MURPHY, J.A.: 'Distortion of a simple Gaussian beam on reflection from off-axis ellipsoidal mirrors', *Int. J. Infrared & Millim. Waves*, 1987, **8**, pp. 1165–1187

8 CHU, TA-SHING: 'Polarisation properties of off-set dual-reflector antennas', *IEEE Trans.*, 1991, **AP-39**, pp. 1753–1756

9 CAHILL, R., and PARKER, E.A.: 'Design of multi-layer frequency selective surfaces', *Microwave Opt. Technol. Lett.*, 1995, **8**, pp. 293–296

10 LESURF, J.: 'Millimetre-wave optics, devices and systems' (Adam Hilger/IOPP, Bristol and New York, 1990)

Received 27th November 1995

Derek Martin is Emeritus Professor of Physics at Queen Mary and Westfield College (Mile End Road, London, E1 4NS) in the University of London. His research interests have been in the development of techniques for the generation, detection and spectral analysis of electromagnetic waves at terahertz frequencies and in the application of those techniques in spectroscopic studies of solids and of stratospheric chemistry, and in the diagnostics of thermonuclear plasmas. He was awarded the K. J. Button Prize by the International Society for Optical Engineering in 1992 and the Metrology Award of the National Physical Laboratory in 1983. He has been Honorary Secretary of the Institute of Physics, Editor of Advances in Physics, and a member of the British National Committee for Physics and of that for Radio Science.

R. J. Martin graduated from the School of Physics, Bath University, in 1982. Since then he has been involved in the field of quasi-optics, initially with QMW Instruments, the technology transfer arm of Queen Mary and Westfield College, University of London, and later with British Aerospace and Matra Marconi Space UK Ltd. He has been responsible for advances in the long-wave optics field, and for designing several systems and components throughout the millimetric and submillimetric range. He is now with Matra Marconi Space UK Ltd., PO Box 16, Filton, Bristol, BS12 7YB, UK.